Recursive nearest agglomeration (ReNA): fast clustering for approximation of structured signals

Andrés Hoyos-Idrobo, Gaël Varoquaux, Jonas Kahn, Bertrand Thirion

Recursive nearest agglomeration (ReNA): fast clustering for approximation of structured signals

Andrés HOYOS-IDROBO, Gaël VAROQUAUX, Jonas KAHN, and Bertrand THIRION

Abstract—In this work, we revisit fast dimension reduction approaches, as with random projections and random sampling. Our goal is to summarize the data to decrease computational costs and memory footprint of subsequent analysis. Such dimension reduction can be very efficient when the signals of interest have a strong structure, such as with images. We focus on this setting and investigate feature clustering schemes for data reductions that capture this structure. An impediment to fast dimension reduction is that good clustering comes with large algorithmic costs. We address it by contributing a linear-time agglomerative clustering scheme, Recursive Nearest Agglomeration (ReNA). Unlike existing fast agglomerative schemes, it avoids the creation of giant clusters. We empirically validate that it approximates the data as well as traditional variance-minimizing clustering schemes that have a quadratic complexity. In addition, we analyze signal approximation with feature clustering and show that it can remove noise, improving subsequent analysis steps. As a consequence, data reduction by clustering features with ReNA yields very fast and accurate models, enabling to process large datasets on budget. Our theoretical analysis is backed by extensive experiments on publicly-available data that illustrate the computation efficiency and the denoising properties of the resulting dimension reduction scheme.

Index Terms—clustering, dimensionality reduction, matrix sketching, classification, neuroimaging, approximation

1 Introduction

CHEAP and ubiquitous sensors lead to a rapid increase of data sizes, in the sample direction –the number of measurements– but also the feature direction –the richness of each measurement. These "big data" put a lot of strain on data management and analysis. Indeed, they entail large memory and storage footprint, and the algorithmic cost of querying or processing them is often super-linear in the data size. Yet, such data often display a structure, for instance originating from the physical process probed by the sensor. This structure implies that the data can be well approximated by a lower-dimensionality representation, dropping drastically the cost of subsequent data management or analysis. The present paper focuses on these fast signal approximations.

The deluge of huge sensor-based data is ubiquitous: in imaging sciences –*eg* biological [1] or medical [2]– in genomics [3], [4], with time series, as in seismology [5]... Researchers have introduced a variety of strategies to mitigate the computational costs created by the rapid increase in signal resolution. Many approaches integrate reduced signal representations in statistical analysis. Super-voxels, leveraging the image structure, accelerate optical flow algorithms for huge biological microscopy images [1]. Fast large-scale image search can use a reduced representation of the images combining mid-level features with the image topology [6]. In genomics, clustering can extract a small number of *candidate* SNPs (single nucleotype polymorphisms) from a large set of SNPs, speeding up subsequent analysis [7], [8]. Using the topology of the DNA strand to restrict this clustering makes it faster and more relevant for genomic studies [8]. Similarly, as medical images exhibit strong spatial structure, clustering [9] or super-voxels [10], [11] are used to speed up statistical analysis. Finally, in the analysis of large seismic time-series [5], building indexes of the database is crucial for fast retrieval of similar waveforms. Dimension reduction is a good strategy for such fast indexing [5], [12], even more so if it captures the signals' structure [13].

In signal processing and machine learning, fast signal approximation is central to speeding up algorithms: approximating kernels [14], fast approximate nearest neighbors [15], or randomized linear algebra [16]. Note that for all these, the only requirement on the reduced representation is that it preserves pairwise distances between signals. For huge datasets, data reduction is very beneficial. First, it reduces memory requirements, and, second, it decreases computation time. Indeed, even for linear complexity algorithms, the computation cost of growing data size is worse than linear: as datasets no longer fit in cache, standard computational architectures cannot be efficiently used.

Here, we are interested in representing *structured* signals, and using this structure to improve the data approximation and speed up its computation. Signal processing often models such signals as generated from a random process acting on a neighborhood structure. Individual features of the data then form vertices of a graph. This structure graph is given by the specificity of the acquisition process, such as the physics of the sensors. Note that such a description is not limited to regular grids, such as time-series or images, and encompasses for instance data on a folded surface [17].

Various approaches are used as standard tools in the literature to compress datasets. Typically, a data matrix is represented by a sketch matrix that is significantly smaller than the original, but approximates it well. Two sketching

- *A. Hoyos-Idrobo, G.Varoquaux and B.Thirion are with Parietal team, Inria, CEA, University Paris-Saclay, 91191, Gif sur Yvette, France. E-mails: firstname.lastname@inria.fr*
- *J. Kahn is with the Institut de Mathématiques de Toulouse, UMR5219, Université de Toulouse, CNRS, France. E-mail: jonas.kahn@math.univ-toulouse.fr*

strategies are common employed: *i)* approximating the matrix by a small subset of its rows (or columns) (e.g. Nyström [18] and CUR [19]); *ii)* randomly combining matrix rows, relying on subspace embedding and strong concentration phenomena, e.g. random projections [20]. Random projections are appealing as they come with theoretical guaranties quantifying the expected distortion. For information retrieval, state-of-the-art indexing of times series can be achieved with a symbolic representation [21] that finds a regular piecewise constant approximation of the signal, and then associates a symbolic code with this quantization.

Here, we seek fast dimension reduction that adapts to common statistics across the data, as with the Nyström approximation, and unlike random projections. Additionally, we want this scheme to account for the graph structure of the data. For this, we use *feature grouping*, approximating a signal with constant values over a partition of features. We use a clustering algorithm to adapt the partition to the data statistics. Agglomerative clustering algorithms are amongst the fastest approaches to extract many clusters with graph-connectivity constraints. However, they fail to create clusters of evenly-distributed size, favoring a few huge clusters[1].

Contributions: in this paper, our contributions are two-fold. *i)* We analyze dimensionality reduction of structured signals by feature grouping. We show that it has a denoising effect on structured signals, hence improves subsequent statistical analysis. *ii)* We introduce a fast agglomerative clustering, that finds clusters of roughly even size in linear time, maintaining meaningful information on the structure of the data. Our pipeline is very beneficial for analysis of large-scale structured datasets, as the dimension reduction is very fast, and it reduces the computational cost of various estimators without losing accuracy.

The paper is organized as follows. In section 2, we give prior art on fast dimension reduction and analyze the theoretical performance of feature grouping. In section 3, we introduce ReNA, a new fast clustering algorithm. In section 4, we carry out extensive empirical studies comparing many fast dimension-reduction approaches and show on real-life data that feature grouping can have a denoising effect.

Notations: Column vectors are written using bold lower-case, e.g., $\mathbf{x}$. For a vector $\mathbf{x}$, the i-th component of $\mathbf{x}$ is denoted $\mathbf{x}_i$. Matrices are written using bold capital letters, e.g., $\mathbf{X}$. The jth column vector of $\mathbf{X}$ is denoted $\mathbf{X}_{*,j}$, the ith row vector of $\mathbf{X}$ is denoted $\mathbf{X}_{i,*}$, and $[n]$ denotes $\{1, \ldots, n\}$. Letters in calligraphic, e.g. $\mathcal{P}$ denotes sets or graphs, and it will be clarified by the context. Let $\{\mathcal{C}_i\}_{i=1}^k$ be short for the set $\{\mathcal{C}_1, \ldots, \mathcal{C}_k\}$. $|\cdot|$ denotes the cardinality of a set. The ℓ_p norm of a vector $\mathbf{x} = [\mathbf{x}_1, \mathbf{x}_2, \ldots, \mathbf{x}_k] \in \mathbb{R}^k$ is defined as $\|\mathbf{x}\|_p = \left(\sum_{i=1}^k |\mathbf{x}_i|^p\right)^{\frac{1}{p}}$, for $p = [1, \infty)$.

2 Dimension reduction of structured signals

In this section, we review useful prior art on random projections and random sampling. Then we analyze signal approximation with feature grouping.

1. This phenomenon is known as percolation in random graphs [22].

2.1 Background and related prior art

Signal approximation with random projections or random sampling techniques is now central to many data analysis, machine learning, or signal processing algorithms.

Let $\mathbf{X} \in \mathbb{R}^{p \times n}$ be a data matrix composed of n samples and p features (i.e. pixels/voxels). We are interested in an operator $\mathbf{\Phi} \in \mathbb{R}^{k \times p}$ that reduces the dimension of the data in the feature direction, acting as a preprocessing step to make further analysis more tractable. This operator should maintain approximately the pairwise distance between pairs of images $(\mathbf{X}_{*,i}, \mathbf{X}_{*,j}) \in \mathbf{X}^2$ for $(i, j) \in [n]^2$,

$$\|\mathbf{\Phi}\, \mathbf{X}_{*,i} - \mathbf{\Phi}\, \mathbf{X}_{*,j}\|_2^2 \approx \|\mathbf{X}_{*,i} - \mathbf{X}_{*,j}\|_2^2, \;\; \forall (i,j) \in [n]^2. \quad (1)$$

Note that this approximation needs to hold only on the data submanifold, and not the entire $\mathbb{R}^p$.

Random projections: A standard choice, is to build $\mathbf{\Phi}$ with random projections, $\mathbf{\Phi}_{\mathsf{RP}}$ [23]. It is particularly attractive due its algorithmic simplicity and theoretical guaranties that make it ϵ-isometric (see Eq. 2).

Lemma 2.1. [20] By the Johnson-Lindenstrauss lemma, the pairwise distances among a collection $\mathcal{X}$ of n-points in $\mathbb{R}^p$ are approximately maintained when the points are mapped randomly to an Euclidean space of dimension $k = O(\epsilon^{-1} \log n)$ up to a distortion at most ϵ. More precisely, given $\epsilon, \delta \in (0, 1)$ and $k \leq p$, there exists a random linear projection $\mathbf{\Phi}_{\mathsf{RP}} : \mathbb{R}^p \to \mathbb{R}^k$ such that for every $\mathbf{x}, \mathbf{x}'$ in $\mathcal{X}$, the following relations hold:

$$(1-\epsilon)\|\mathbf{x}-\mathbf{x}'\|_2^2 \leq \|\mathbf{\Phi}_{\mathsf{RP}}\, \mathbf{x} - \mathbf{\Phi}_{\mathsf{RP}}\, \mathbf{x}'\|_2^2 \leq (1+\epsilon)\|\mathbf{x}-\mathbf{x}'\|_2^2, \quad (2)$$

with probability at least $1 - \delta$.

These Johnson-Lindenstrauss embeddings have been widely used in the last years. By providing a low-dimensional representation of the data, they can speed up algorithms dramatically, in particular when their run time depends super-linearly on the dimension of the data. In addition, as this representation of the data is accurate in the sense of the ℓ_2 norm, it can be used to approximate shift-invariant kernels [24] [14].

The $\mathbf{\Phi}_{\mathsf{RP}}$ matrix can be generated by sampling from a Gaussian distribution with rescaling. In practice, a simple and efficient generation scheme can yield a very sparse random matrix with good properties [25]. The computational performance of random projections can be further improved *i)* with fast orthogonal decompositions [15] [26], *ii)* by reducing the number of necessary projections when the data lie on a submanifold of $\mathbb{R}^p$ [27].

This approach suffers from two important limitations: *i)* inverting the random mapping from $\mathbb{R}^p$ to $\mathbb{R}^k$ is difficult, requiring more constraints on the data (e.g. sparsity), which entails another estimation problem. As a result, it yields less meaningful or easily interpretable results, as the ensuing inference steps cannot be made explicit in the original space. *ii)* This approach is suboptimal for structured datasets, since it ignores the properties of the data, such as a possible spatial continuity.

Random sampling: A related technique is random sampling, and in particular the Nyström approximation method. This method is mainly used to build a low-rank approximation of a matrix. It is particularly useful with

kernel-based methods when the number n of samples is large, given that the complexity of building a kernel matrix is at least quadratic in n [28]. It has become a standard tool when dealing with large-scale datasets [18].

The idea is to preserve the spectral structure of a kernel matrix $\mathbf{K}$ using a subset of columns of this matrix, yielding a low-rank approximation. This can be cast as building a data-driven feature mapping $\mathbf{\Phi}_{\text{Nys}} \in \mathbb{R}^{k\times p}$. In a linear setting, the kernel matrix is defined as $\mathbf{K} = \mathbf{X}^\mathsf{T}\,\mathbf{X}$, which leads to the following approximation:

$$\mathbf{K}_{i,j} = \langle \mathbf{X}_{*,i}, \mathbf{X}_{*,j} \rangle \approx \langle \mathbf{\Phi}_{\text{Nys}}\,\mathbf{X}_{*,i}, \mathbf{\Phi}_{\text{Nys}}\,\mathbf{X}_{*,j} \rangle\,. \qquad (3)$$

Here, building a base $\mathbf{\Phi}_{\text{Nys}}$ is achieved by randomly sampling $k \ll n$ points from $\mathbf{X}$, and then normalizing them –i.e. whitening the subsampled data– see algorithm 2 in supplementary materials The cost of the SVD dominates the complexity of this method $O(pk\min\{p,k\})$. This method is well suited for signals with a common structure, for instance images that share a common spatial organization captured by $\mathbf{\Phi}_{\text{Nys}}$. As the Nyström approximation captures the structure of the data, it can also act as a regularization [29].

2.2 Dimension reduction by feature grouping

Here we analyze feature grouping for signal approximation.

2.2.1 The feature-grouping matrix and approximation

Feature grouping defines a matrix $\mathbf{\Phi}$ that extracts piece-wise constant approximations of the data [30]. Let $\mathbf{\Phi}_{\text{FG}}$ be a matrix composed with constant amplitude groups (clusters). Formally, the set of k clusters is given by $\mathcal{P} = \{\mathcal{C}_1, \mathcal{C}_2, \ldots, \mathcal{C}_k\}$, where each cluster $\mathcal{C}_q \subset [p]$ contains a set of indexes that does not overlap other clusters, $\mathcal{C}_q \cap \mathcal{C}_l = \emptyset$, for all $q \neq l$. Thus, $(\mathbf{\Phi}_{\text{FG}}\,\mathbf{x})_q = \alpha_q \sum_{j\in\mathcal{C}_q} \mathbf{x}_j$ yields a reduction of a data sample $\mathbf{x}$ on the q-th cluster, where α_q is a constant for each cluster. With an appropriate permutation of the indexes of the data $\mathbf{x}$, the matrix $\mathbf{\Phi}_{\text{FG}}$ can be written as

$$\mathbf{\Phi}_{\text{FG}} = \begin{bmatrix} \alpha_1\text{—}\alpha_1 & 0\text{—}0 & \ldots & 0\text{—}0 \\ 0\text{—}0 & \alpha_2\text{—}\alpha_2 & \ldots & 0\text{—}0 \\ \vdots & \vdots & \ddots & \vdots \\ 0\text{—}0 & 0\text{—}0 & \ldots & \alpha_k\text{—}\alpha_k \end{bmatrix} \in \mathbb{R}^{k\times p}.$$

We choose $\alpha_q = 1/\sqrt{|\mathcal{C}_q|}$ to set the non-zero singular values of $\mathbf{\Phi}_{\text{FG}}$ to 1, making it an orthogonal projection.

We call $\mathbf{\Phi}_{\text{FG}}\,\mathbf{x} \in \mathbb{R}^k$ the *reduced* version of $\mathbf{x}$ and $\mathbf{\Phi}_{\text{FG}}^\mathsf{T}\mathbf{\Phi}_{\text{FG}}\,\mathbf{x} \in \mathbb{R}^p$ the *approximation* of $\mathbf{x}$. Note that having an approximation of the data means that the ensuing inference steps can be made explicit in the original space. As the matrix $\mathbf{\Phi}_{\text{FG}}$ is sparse, this approximation follows the same principle as [31], speeding up computational time and reducing memory storage.

Let $M(\mathbf{x})$ be the approximation error for a data $\mathbf{x}$ given a feature grouping matrix $\mathbf{\Phi}_{\text{FG}}$,

$$M(\mathbf{x}) = \left\| \mathbf{x} - \mathbf{\Phi}_{\text{FG}}^\mathsf{T}\mathbf{\Phi}_{\text{FG}}\,\mathbf{x} \right\|_2^2, \qquad (4)$$

this is often called inertia in the clustering literature. This corresponds to the sum of all the local errors (the approximation error for each cluster), $M(\mathbf{x}) = \sum_{q=1}^k m_q$, where $m_q(\mathbf{x})$ is the sum of squared differences between the values in the q-th cluster and its representative center, as follows

$$m_q(\mathbf{x}) = \left\| \mathbf{x}_{\mathcal{C}_q} - \frac{(\mathbf{\Phi}_{\text{FG}}\,\mathbf{x})_q}{\sqrt{|\mathcal{C}_q|}} \right\|_2^2, \qquad (5)$$

where $\mathbf{x}_{\mathcal{C}_q}$ are the values $\mathbf{x}_i$ such that $i \in \mathcal{C}_q$. The squared norm of the data $\mathbf{x}$ is then decomposed in two terms: fidelity and inertia, taking the form (see section 2 in supplementary materials):

$$\|\mathbf{x}\|_2^2 = \underbrace{\|\mathbf{\Phi}_{\text{FG}}\,\mathbf{x}\|_2^2}_{\text{Reduced norm}} + \underbrace{\sum_{q=1}^k \left\| \mathbf{x}_{\mathcal{C}_q} - \frac{(\mathbf{\Phi}_{\text{FG}}\,\mathbf{x})_q}{\sqrt{|\mathcal{C}_q|}} \right\|_2^2}_{M(\mathbf{x})\text{: Inertia}}. \qquad (6)$$

Eq. 6 is key to understanding the desired properties of a matrix $\mathbf{\Phi}_{\text{FG}}$. In particular, it shows that it is beneficial to work in a large k regime to reduce the inertia.

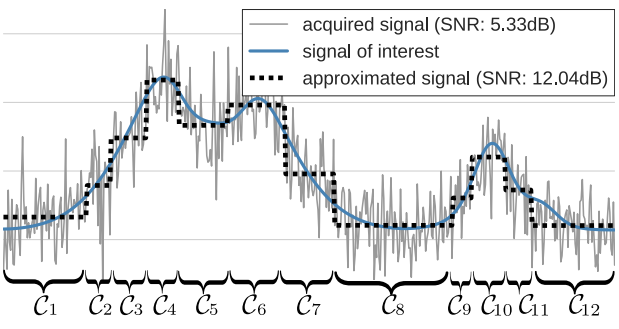

Figure 1. **Illustration of the approximation of a signal:** Piece-wise constant approximation of a 1D signal contaminated with additive Gaussian noise $\mathbf{x} \in \mathbb{R}^{512}$. The approximated signal is represented as $\mathbf{\Phi}_{\text{FG}}^\mathsf{T}\mathbf{\Phi}_{\text{FG}}\,\mathbf{x}$, where the matrix $\mathbf{\Phi}_{\text{FG}} \in \mathbb{R}^{12\times 512}$ is built using the clustering of the intensities with a spatial constraint (i.e. spatially-constrained Ward clustering). Only 12 clusters can preserve the structure of the signal and decrease the noise, as seen from the . signal-to-noise-ratio (dB).

2.2.2 Capturing signal structure

We consider data with a specific structure, e.g. spatial data. Well-suited dimensionality reduction can leverage this structure to bound the approximation error. We assume that the data $\mathbf{x} \in \mathbb{R}^p$ are generated from a process acting on a space with a neighborhood structure (topology). To encode this structure, the data matrix $\mathbf{X}$ is associated with an undirected graph $\mathcal{G}$ with p vertices $\mathcal{V} = \{v_1, v_2, \ldots, v_p\}$. Each vertex of the graph corresponds to an index in the data matrix $\mathbf{X}$ and the presence of an edge means that these features are connected. For instance, for 2D or 3D image data, the graph is a 2D or 3D lattice connecting neighboring pixels. The graph defines a graph distance between features $\text{dist}_\mathcal{G}$. In practice, we perform the calculations with the adjacency matrix $\mathbf{G}$ of the graph $\mathcal{G}$.

Definition 2.1. **L-Smoothness of the signal:** A signal $\mathbf{x} \in \mathbb{R}^p$ structured by a graph $\mathcal{G}$, is pairwise Lipschitz smooth

with parameter L when it satisfies

$$|\mathbf{x}_i - \mathbf{x}_j| \leq L \operatorname{dist}_{\mathcal{G}}(v_i, v_j), \quad \forall (i,j) \in [p]^2. \tag{7}$$

This definition means that the signal is smooth with respect to the graph that encodes the underlying structure. Note that $\operatorname{dist}_{\mathcal{G}}$ has no unit since the scale is fixed by having each edge have length 1.

Lemma 2.2. Let $\mathbf{x} \in \mathbb{R}^p$ be a pairwise L-Lipschitz signal, and $\mathbf{\Phi}_{\mathsf{FG}} \in \mathbb{R}^{k \times p}$ be a fixed feature grouping matrix, formed by $\{\mathcal{C}_1, \ldots, \mathcal{C}_k\}$ clusters. Then the following holds:

$$\|\mathbf{x}\|^2 - L^2 \sum_{q=1}^{k} |\mathcal{C}_q| \operatorname{diam}_{\mathcal{G}}(\mathcal{C}_q)^2 \leq \|\mathbf{\Phi}_{\mathsf{FG}}\, \mathbf{x}\|^2 \leq \|\mathbf{x}\|^2, \tag{8}$$

where $\operatorname{diam}_{\mathcal{G}}(\mathcal{C}_q) = \sup_{v_i, v_j \in \mathcal{C}_q} \operatorname{dist}_{\mathcal{G}}(v_i, v_j)$.

See section 2 in supplementary materials for a proof.

We see that the approximation is better if: *i)* the cluster sizes are about the same, and *ii)* the clusters have a small diameter. These arguments are based only on the assumption of smoothness of the signal. Refining Eq.8 gives an intuition on how a partition could be adapted to the data:

Corollary 2.1. Let L_q be the smoothness index inside cluster C_q, for all $q \in [k]$. This is the minimum L_q such that:

$$|\mathbf{x}_i - \mathbf{x}_j| \leq L_q \operatorname{dist}_{\mathcal{G}}(v_i, v_j), \quad \forall (i,j) \in C_q^2.$$

Then the following two inequalities hold:

$$\begin{aligned} \|\mathbf{x}\|_2^2 - \sum_{q=1}^{k} |\mathcal{C}_q| \sup_{\mathbf{x}_i, \mathbf{x}_j \in \mathbf{x}_{\mathcal{C}_q}} |\mathbf{x}_i - \mathbf{x}_j|_2^2 \leq \\ \|\mathbf{x}\|_2^2 - \sum_{q=1}^{k} L_q^2 |\mathcal{C}_q| \operatorname{diam}_{\mathcal{G}}(\mathcal{C}_q)^2 \leq \|\mathbf{\Phi}_{\mathsf{FG}}\, \mathbf{x}\|_2^2. \end{aligned} \tag{9}$$

We can see that the approximation is better if: *i)* the signal in a cluster is homogeneous (low L_q); *ii)* clusters in irregular areas (high L_q) are smaller.

Clusters $\mathcal{P}$ of the graph $\mathcal{G}$ can be seen as connected components of a subgraph. In this context, the size of the largest group, $\max_{q \in [k]} |\mathcal{C}_q|$, can be studied with percolation theory, that characterizes the appearance of a giant connect component as edges are added [22].

2.2.3 *Approximating signals with unstructured noise*

We consider an additive noise model: the acquired data $\mathbf{X}$ is a spatially-structured signal of interest $\mathbf{S}$ contaminated with by unstructured noise $\mathbf{N}$,

$$\mathbf{X}_{*,i} = \mathbf{S}_{*,i} + \mathbf{N}_{*,i}, \quad \forall i \in [n]. \tag{10}$$

When the feature grouping matrix $\mathbf{\Phi}_{\mathsf{FG}}$ is applied to the acquired signal, the noise will be reduced (via within-cluster averaging). In particular, for an i.i.d. noise with zero-mean and variance σ^2, we have the following relation between the Mean Squared Error of the approximated data, $\mathrm{MSE}_{\mathrm{approx}}$, and the non-reduced one $\mathrm{MSE}_{\mathrm{orig}}$ (see section 3 in supplementary materials):

$$\mathrm{MSE}_{\mathrm{approx}} \leq L^2 \sum_{q=1}^{k} |\mathcal{C}_q| \operatorname{diam}_{\mathcal{G}}(\mathcal{C}_q)^2 + \frac{k}{p} \mathrm{MSE}_{\mathrm{orig}}. \tag{11}$$

We will have a denoising effect if the smoothness parameter satisfies

$$L^2 \leq \frac{(p-k)}{\sum_{q=1}^{k} |\mathcal{C}_q| \operatorname{diam}_{\mathcal{G}}(\mathcal{C}_q)^2}\, \sigma^2. \tag{12}$$

When the signal of interest is smooth enough and the cluster sizes are roughly even, the feature grouping will reduce the noise, preserving the information of the low-frequency signal $\mathbf{S}_i$. Fig. 1 presents a graphical illustration of the reduction and denoising capabilities of feature grouping.

The challenge is then to define a good $\mathbf{\Phi}_{\mathsf{FG}}$, given that data-unaware feature partitions are sub-optimal, as they do not respect the underlying structures and lead to signal loss.

3 ReNA: A fast structured clustering algorithm

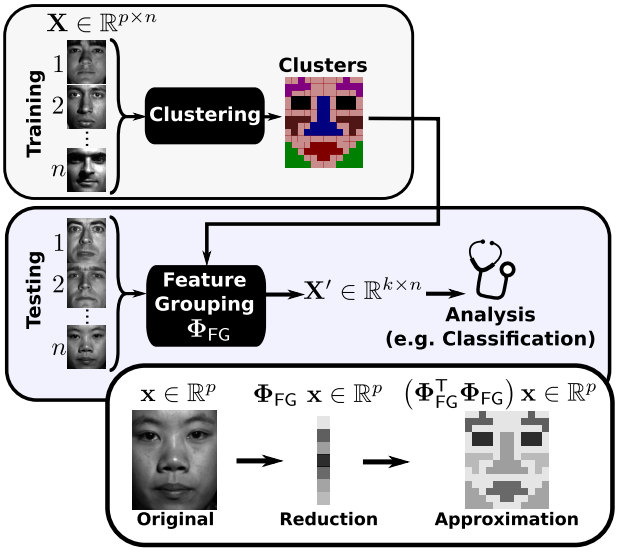

Figure 2. **Feature grouping for statistical analysis of structured images:** Illustration of rhe different steps of feature grouping-based data approximation . The approach consists in finding a data-driven spatial reduction $\mathbf{\Phi}_{\mathsf{FG}}$ using clustering. Then, the data $\mathbf{x}$ are reduced to $\mathbf{\Phi}_{\mathsf{FG}}\, \mathbf{x}$ and then used for further statistical analysis (e.g. classification).

In the feature-grouping setting above, we now consider a data-driven approach to build the matrix $\mathbf{\Phi}_{\mathsf{FG}}$. We rely on feature clustering: a clustering algorithm is used to define the groups of feature from the data. $\mathbf{X} \in \mathbb{R}^{p \times n}$ is represented by a reduced version $\mathbf{\Phi}_{\mathsf{FG}}\, \mathbf{X}$, where p is potentially very large (greater than 100 000), whereas k is smaller but close enough to p (e.g. $k = \lfloor p/20 \rfloor$). As illustrated in Fig 2, Once the reduction operator $\mathbf{\Phi}_{\mathsf{FG}}$ has been learned, it can be applied to new data.

3.1 Existing fast clustering algorithms

K-means clustering is a natural choice as it minimizes the total inertia in Eq.6. But it tends to be expensive in our setting: The conventional k-means algorithm has a complexity of $O(n\,k)$ per iterations [32]. However, the larger the number of clusters, the more iterations are needed to converge, and the worst case complexity is given[2] by $O(p^{k+2/n})$ [33]. This complexity becomes prohibitive with many clusters.

2. Note that here n and p are swapped compared to common clustering literature, as we are doing *feature* clustering.

Super-pixel approaches: In computer vision, feature clustering can be related to the notion of *super-pixels* (super-voxels for 3D images). The most common fast algorithm for super-pixels is SLIC [32], which has a low computational cost and produces super-pixels/super-voxels of roughly even sizes. SLIC performs a local clustering of the image values with a spatial constrain, using as a distance measure the combination of two Euclidean distances: image values and spatial positions. The SLIC algorithm is related to K-means, but it performs a fixed small number of iterations, resulting in a complexity of $O(np)$. Its main drawback is that, in the large-k regime, it can be difficult to control precisely the number of clusters, as some clusters often end up empty in the final assignment.

Agglomerative clustering: Agglomerative clustering algorithms are fast in the setting of a large number k of clusters. Unlike most clustering algorithms, adding a graph structure constraint makes them even faster, as they can then discard association between non-connected nodes.

Agglomerative clustering schemes start off by placing every data element in its own cluster, then they proceed by merging repeatedly the closest pair of clusters until finding the desired number of clusters [34]. Various methods share the same approach, differing only in the linkage criterion used to identify the clusters to be merged. The most common linkages are single, average, complete [34] and Ward [35]. Average-linkage, complete-linkage, and Ward are generally preferable over single-linkage, as they tend to yield more balanced clusters. Yet single-linkage clustering is often used as it is markedly faster; it can be obtained via a Minimum Spanning Tree and has a complexity of $O(np + p \log p)$ [36]. Average-linkage, complete-linkage and Ward have a worts case complexity of $O(np^2)$ [36].

The approximation properties of feature grouping are given by the distribution of cluster sizes (Eq. 6). Balanced clusters are preferable for low errors. Nevertheless, agglomerative clustering on noisy data can often lead to a "preferential attachment" behavior, where large clusters grow faster than smaller ones. In this case, the largest cluster dominates the distortion, as in Lemma. 2.2. By considering that the clusters are connected components on a similarity graph, this behavior can be linked to percolation theory [22], that characterizes the appearance of a giant connected component (i.e. a huge cluster). In this case, the clustering algorithm is said to *percolate*, and thus cannot yield balanced cluster sizes.

In brief, single-linkage clustering is fast but suffers form percolation issues [37] and Ward's algorithm performs often well in terms of goodness of fit for large k [38].

More sophisticated agglomerative strategies have been proposed in the framework of computer vision (e.g. [39]), but they have not been designed to avoid percolation and do not make it possible to control the number k of clusters.

3.2 Contributed clustering algorithm: ReNA

For feature clustering on structured signals, an algorithm should take advantage of the generative nature of the data, e.g. for images, work with local image statistics. Hence we rely on neighborhood graphs [40].

Neighborhood graphs form an important class of geometric graphs with many applications in signal processing, pattern recognition, or data clustering. They are used to model local relationships between data points, with ϵ-neighborhood graphs[3] or k-nearest neighbor graphs.

The ϵ-nearest neighbor graph is the core of one of the most popular scalable clustering algorithms, DBSCAN [41]. It is a density-based clustering method for which the number k of clusters is implicitly set by the ϵ neighborhood's radius. Its main drawback is its high sensitivity to the choice of this very parameter. K-nearest neighbor graphs, on the other hand, are not well suited for clustering as they tend to percolate for k greater than or equal to 2. In contrast, the 1-nearest neighbor graph (1-NN) is not likely to percolate [42]. For this reason, we use the 1-NN graph.

In a nutshell, our algorithm relies on extracting the connect components of a 1-NN graph. To reach the desired number k of clusters, we apply it recursively. The algorithm outline is as follows:

Initialization: We start by placing each of the p features of the data $\mathbf{X}$ in its own cluster $\mathcal{P} = \{\mathcal{C}_1, \ldots, \mathcal{C}_p\}$. We use the binary adjacency matrix $\mathbf{G} \in \mathbb{R}^{p \times p}$ of the graph $\mathcal{G}$, that encodes the topological structure of the features.

Nearest neighbor grouping: We use the nearest neighbor of a similarity graph as linkage criterion. We then extract the connected components of this subgraph to reduce the data matrix $\mathbf{X}$ and the topological structure $\mathbf{G}$. These operations are summarized in the next steps:

1) **Graph representation:** We build the similarity graph $\mathcal{D}$ of the data $\mathbf{X}$, represented by the adjacency matrix $\mathbf{D} \in \mathbb{R}^{p \times p}$. The weights are constrained by $\mathbf{G}$[4].
2) **Finding 1-NN:** Creating a 1-nearest neighbor graph $\mathcal{Q}$, represented by the adjacency matrix $\mathbf{Q} \in \mathbb{R}^{p \times p}$, where each vertex of $\mathcal{D}$ is associated with its nearest neighbor in the sense of the dissimilarity measure.
3) **Getting the clusters:** We use [43] to extract the set of connected components of $\mathbf{Q}$ and assign them to the new set of clusters $\mathcal{P}$.
4) **Reduction step:** The clusters are used to reduce the graph $\mathbf{G}$ and the data $\mathbf{X}$.

Stopping condition: Nearest neighbor grouping can be performed repeatedly on the reduced versions of the

3. ϵ-neighborhood graph: v_i and v_j are connected if $\|v_i - v_j\| \leq \epsilon$.
4. This corresponds to an element-wise condition, where a similarity weight is assigned only if the edges are connected according to $\mathbf{G}$.

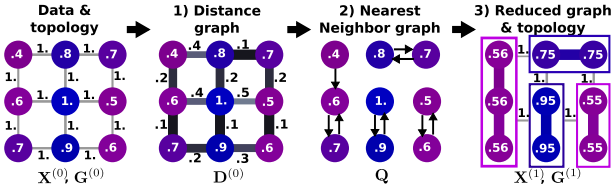

Figure 3. **The nearest neighbor grouping:** The algorithm receives a data matrix $\mathbf{X}$ represented on a regular square lattice $\mathbf{G}$. *left)* The nodes correspond to the feature values and the edges are the encoded topological structure. *1) Graph representation:* We calculate the similarity matrix $\mathbf{D}$. *2) Finding 1-NN:* We proceed by finding the 1-nearest neighbors subgraph $\mathbf{Q}$ according to the similarity measure. *3) Getting the clusters and reduction step:* We extract the connected components of $\mathbf{Q}$ and merge the connected nodes.

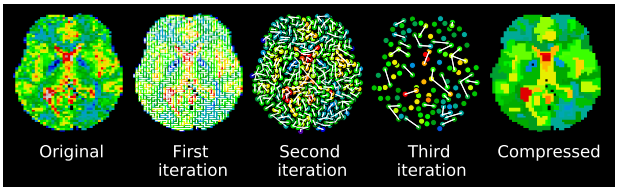

Figure 4. **Illustration of the working principle of the Recursive Nearest Neighbor, ReNA:** The white lines represent the edges of the graph. The algorithm receives the original image, considering each feature (i.e. pixel or voxel in the image) as a cluster. From now on, for each iteration, the nearest clusters are merged, yielding a reduced graph, until the desired number of clusters is found.

graph $\mathbf{G}$ and the data $\mathbf{X}$ until the desired number k of clusters is reached[5].

Fig.3 presents one iteration of the nearest neighbor grouping on a regular square lattice. The pseudo-code of ReNA is given in algorithm 1 and an illustration on a 2D brain image in Fig.4.

The algorithm is iterated until the desired number of clusters k is reached[6]. As the number of vertices is divided by 2 at each step, the number of iterations is at most $O\{\log(p/k)\}$; in practice, we never have to go beyond 5 iterations. The cost of computing similarities is linear in n and, as all the operations involved are also linear in the number of vertices p, the total procedure is $O(np)$.

4 Experimental Study

In this section, we conduct a series of experiments to assess the quality of the dimensionality reduction scheme and its viability as a preprocessing step for several statistical analyses. Table. 1 gives a summary of the datasets.

We investigate the performance of feature grouping with a variety of cluster algorithms: single-linkage, average-linkage, complete-linkage, Ward, SLIC, and ReNA. We compare them to other fast dimensionality reductions: random projections, random sampling, as well as image downsampling. We measure their ability to represent the data and characterize their percolation behavior when it is relevant. To evaluate their denoising properties, we use them in prediction tasks. We study not only ℓ_2 methods, but also methods relying on higher moments of the data distribution: ℓ_1 penalization and independent component analysis (ICA).

To present the results, we use the fraction of the signal, which is defined as the ratio between the number k of components and the greatest possible value of k. Here, we have two cases: *i)* for random projections and feature grouping methods, the maximum value of k corresponds to the number p of features, $k/p \times 100\%$; *ii)* for random sampling, the maximum value of k is the number of samples, $k/n \times 100\%$. Downsampling the images with linear interpolation can be seen as using data-independent clusters, all of the same size.

5. In practice the size of the matrices $\mathbf{X}^{(t)}, \mathbf{D}^{(t)}, \mathbf{G}^{(t)}$ decreases during the iterations. Therefore it is necessary to express the partition $\mathcal{P}$ on a reduced index set. To simplify notations, we have not detailed this operation in the algorithm.

6. At each iteration, a connected components routine extracts them from $\mathbf{Q}$ and returns them as a set of clusters $\mathcal{P}$. In the last iteration of the algorithm, if there are less than k connected components, $\mathbf{Q}$ is pruned of its edges with smallest edge values to keep only the $q-k$ shortest edges, so that no less than k components are formed.

Algorithm 1 Recursive nearest neighbor (ReNA) clustering

Require: Data $\mathbf{X} \in \mathbb{R}^{p \times n}$, sparse matrix $\mathbf{G} \in \mathbb{R}^{p \times p}$ representing the associated connectivity graph structure, nearest-neighbor subgraph extraction function NN, connected components extraction function ConnectComp [43], desired number k of clusters.

Ensure: Clustering of the features $\mathcal{P} = \{\mathcal{C}_1, \mathcal{C}_2, \ldots, \mathcal{C}_k\}$

$q = p$ {Initializing the number of clusters to p}
$t = 0$
$\mathbf{X}^{(t)} = \mathbf{X}$
$\mathbf{G}^{(t)} = \mathbf{G}$
while $q > k$ **do**
  $\mathbf{D}^{(t)}_{i,j} \leftarrow \mathbf{G}^{(t)}_{i,j} \|\mathbf{X}^{(t)}_{i,*} - \mathbf{X}^{(t)}_{j,*}\|_2^2,\ (i,j) \in [q]^2$
  {Create a similarity weighted graph.}
  $\mathbf{Q} \leftarrow \mathrm{NN}(\mathbf{D}^{(t)})$ {1-nearest neighbor graph.}
  $\mathcal{P} \leftarrow \mathrm{ConnectComp}(\mathbf{Q})$, [6]
  {Sets of connected components of 1-nearest neighbor graph.}
  $\mathbf{U}_{i,j} \leftarrow \begin{cases} 1 & \text{if } i \in \mathcal{C}_j \\ 0 & \text{otherwise} \end{cases}, (i,j) \in [q] \times [|\mathcal{P}|]$
  {Assignment matrix}
  $\mathbf{X}^{(t+1)} \leftarrow (\mathbf{U}^\mathsf{T}\mathbf{U})^{-1}\mathbf{U}^\mathsf{T}\mathbf{X}^{(t)},\ \mathbf{X}^{(t+1)} \in \mathbb{R}^{|\mathcal{P}| \times n}$
  {Reduced data matrix. Note that the computation boils down to sample averages}
  $\mathbf{G}^{(t+1)} \leftarrow \mathrm{support}(\mathbf{U}^\mathsf{T}\mathbf{G}^{(t)}\mathbf{U}),\ \mathbf{G}^{(t+1)} \in \mathbb{R}^{|\mathcal{P}| \times |\mathcal{P}|}$
  {Reduced between-cluster topological model; the non-zero values are then replaced by ones.}
  $q = |\mathcal{P}|$ {Update the number of clusters}
  $t = t + 1$
end while
return $\mathcal{P}$

4.1 datasets

4.1.1 *Synthetic data*

We generate a synthetic data set composed of 1 000 3D images with and without noise. Each one is a cube of $p = 50^3$ voxels containing a spatially smooth random signal (FWHM=8 voxels), which is our signal of interest $\mathbf{X}$. The acquired signal $\mathbf{S}$ is our signal of interest contaminated by zero-mean additive white Gaussian noise, with a Signal-to-Noise Ratio (SNR) of $2.06dB$.

4.1.2 *The extended Yale B face recognition dataset*

This dataset was designed to study illumination effects on face recognition [44] and consists of $n = 2\,414$ images of 38 identified individuals under 64 lighting conditions. Each image was converted to grayscale, cropped, and normalized to 192×168, leaving $p = 32\,256$ features. For the face recognition task, there are 38 classes, one per subject.

4.1.3 *The Open Access Series of Imaging Studies (OASIS)*

The OASIS dataset[7] [45] consists of anatomical brain images (Voxel Based Morphometry) of 403 subjects. These images were processed with the SPM8 software to obtain modulated grey matter density maps realigned to the MNI

7. OASIS was supported by grants P50 AG05681, P01 AG03991, R01 AG021910, P50 MH071616, U24 RR021382, R01 MH56584.

Table 1
Summary of the datasets and the tasks performed with them.

Dataset	Description	n	p	Task
Synthetic	Cube	10	$\{8, 16, 64, 128\}^3$	Time complexity
		1 000	240 000	Distortion
Faces [44]	Grayscale face images	2 414	32 256	Recognition of 38 subjects
OASIS [45]	Anatomical brain images	403	140 398	Gender discrimination
				Age prediction
HCP [2]	Functional brain images	8 294	254 000	Predicting 17 cognitive tasks
				Spatial ICA

reference template [46] with a 2mm resolution. Finally, the images were masked with a gray-matter mask, which yields about $p = 140\,398$ voxels and 1 GB of dense data. We perform two prediction tasks with this dataset: *i)* Gender classification and *ii)* age regression.

4.1.4 Human Connectome Project (HCP)

We use a functional Magnetic Resonance Imaging (fMRI) dataset from the Human Connectome Project (HCP) [2]. It contains 500 participants (13 removed for quality reasons), acquired at rest –typically analyzed via ICA– and during cognitive tasks [47] –typically analyzed with linear models. We use the HCP minimally preprocessed pipeline [48], resampled at 2mm resolution.

Task-related data: The tasks relate to different cognitive labels on working memory/cognitive control processing.

Resting-state data: We use the two resting-state sessions from 93 subjects. Each session represents about 1GB of data, with $p \approx 220\,000$ and $n = 1\,200$, totaling 200 GB of dense data for all subjects and sessions.

4.2 Technical Aspects

We use scikit-learn for machine-learning tasks (logistic and Ridge regression), fast-ICA, clustering and sparse random projections [49]. We rely on scikit-image for SLIC [50], and on Nilearn to handle neuroimaging data.

Code for ReNA and experiments is available online[8].

4.3 Quality assessment experiments

We perform experiments to measure distortion properties and computation times of the dimensionality reduction methods.

4.3.1 Empirical computational complexity

We empirically assess the scalability of the algorithms as function of the input size. The test is carried out for a synthetic dataset composed of 10 cubes. We varied their dimension $p \in \{8, 16, 64, 128\}^3$ and fix the number of clusters to $k = \lfloor \frac{p}{20} \rfloor$. We repeat 10 times, and report the average computation time.

Fig.5 reports the computation time to estimate $\mathbf{\Phi}$ for the different approximation schemes. It shows that Nyström, single-linkage, complete-linkage, SLIC and ReNA have a behavior linear in the number p of features. Random projections, average-linkage and Ward display a sub-quadratic time complexity, whereas downsampling has a sub-linear behavior. Single-linkage and ReNA outperform other agglomerative methods, reducing the computation time by a factor of 10. Profiling random projections reveals that its run time is dominated by the random number generation. The scikit-learn implementation uses a Mersenne Twister algorithm, with good entropic properties to the cost of increased computations [51].

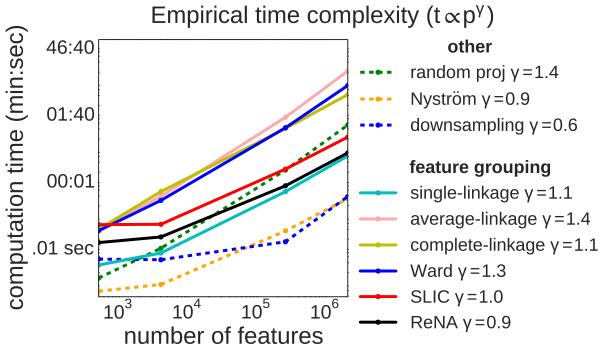

Figure 5. **Complexity of the computation time on a synthetic dataset:** Evaluation of the time complexity to find $\mathbf{\Phi}$ per algorithm on a synthetic data cube, for various feature space dimensions $p \in \{8, 16, 64, 128\}^3$ and fixing the number of clusters to $k = \lfloor \frac{p}{20} \rfloor$. Downsampling displays a sub-linear time complexity, whereas Nyström, single-linkage, complete-linkage, SLIC and ReNA present a linear behavior. Complete-linkage, Ward and random projections have a sub-quadratic time behavior.

4.3.2 Evaluating feature grouping properties

We evaluate the performance of $\mathbf{\Phi}$ with three measures: *i)* The computation time when varying the number of clusters k for a fixed dimension p, *ii)* the signal distortion for various number of clusters; *iii)* the size of the largest cluster. Tuning dimensionality reduction to the data at hand may capture noise in addition to signal. Hence we apply the learned $\mathbf{\Phi}$ on left-out data, in a cross-validation scheme splitting the data randomly 50 times. Each time, we extract the clustering on half of the noisy data and apply it to the other half to measure distortion with regards to the non-noisy signal. We vary the number of clusters $k \in [0.01p, p]$, because all the tested algorithms worked properly in this range. In particular, the implementation used for SLIC [50] posed problems

8. https://github.com/ahoyosid/ReNA

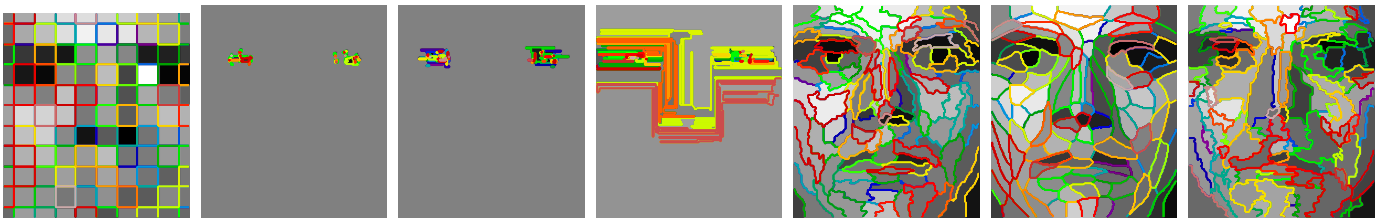

(a) downsampling (b) single-linkage (c) average-linkage (d) complete-linkage (e) Ward (f) SLIC (g) ReNA

Figure 6. **Example of clusters obtained for the extended Yale B face dataset using various feature grouping schemes:** Clusters found on the faces images ($k = 120$). Single, average and complete linkage clustering fail to represent the spatial structure of the data, finding a huge cluster leaving only small islands apart. Downsampling fails to capture the global appearance. In contrast, methods yielding balanced clusters maintain this structure. Colors are random.

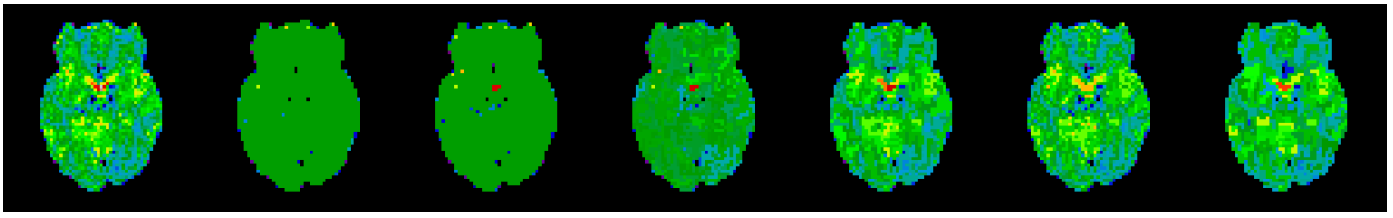

(a) Original (b) single-linkage (c) average-linkage (d) complete-linkage (e) Ward (f) SLIC (g) ReNA

Figure 7. **Approximation of an MRI image obtained with various feature grouping algorithms:** A compressed representation of an MRI image (slice) using various clustering methods for a number of clusters $k = 1000$. Traditional agglomerative clustering methods exhibit giant clusters, loosing meaningful information. In contrast, Ward, SLIC and ReNA algorithms present a better performance, finding balanced clusters.

to control the number of clusters in a larger regime. For the Nyström approximation, we vary the dimensionality $k \in [0.01n, n]$.

The clusters found by the clustering algorithms on the faces dataset are shown on Fig.6. We can see that single, average, and complete linkage have percolated, failing to retain the spatial structure of the faces. Downsampling also fails to capture this structure, while Ward, SLIC and ReNA perform well in this task. Additionally, Fig. 7 shows the approximations of brain images using clustering methods. As previously, percolating algorithms fail to represent spatial features of the data.

Distortion: We want to test whether the reduction $\mathbf{\Phi}\,\mathbf{X}$ of the noisy data is true to the uncorrupted signal $\mathbf{S}$ (for a full description see section 4 in supplementary materials) ,

$$\|\mathbf{\Phi}\,\mathbf{X}_{*,i} - \mathbf{\Phi}\,\mathbf{X}_{*,j}\|_2 \approx \|\mathbf{S}_{*,i} - \mathbf{S}_{*,j}\|_2,\ \forall (i,j) \in [n]^2. \quad (13)$$

To do so, we split the uncorrupted data matrix $\mathbf{S}$ and the acquired noisy data matrix $\mathbf{X}$ into a train and test sets, $(\mathbf{S}^{\text{train}}, \mathbf{S}^{\text{test}})$ and $(\mathbf{X}^{\text{train}}, \mathbf{X}^{\text{test}})$, randomly selecting half of data for training and the other half for testing. We find a matrix $\mathbf{\Phi}$ using the training set of noisy data, $\mathbf{X}^{\text{train}}$. Then, we measure the pairwise distance between different samples of uncorrupted test data matrix, $\mathbf{S}^{\text{trest}}$, and the pairwise distance between samples of noisy test data after dimensionality reduction, $\mathbf{\Phi}\,\mathbf{X}^{\text{trest}}$. Finally, we measure the relative distortion between these two distances.

This experiment is carried out on two datasets: *i)* Synthetic data, and *ii)* brain activation images (motor tasks) from the HCP dataset.

The results on the distortion behavior are presented in Fig.8 (*top*). Note that SLIC displays an early stopping due the its inability to control the number of clusters. In synthetic data, the clustering methods based on first order linkage criteria (single, average, complete linkage) fail to represent the data accurately. By contrast, SLIC, Ward and ReNA achieve the best representation performance. These methods also show an expected denoising effect inside the useful fraction of the signal value ($k = \{\lfloor p/20 \rfloor, \lfloor p/10 \rfloor\}$), whereby the learned approximation matches approximately the smoothing kernel that characterizes the input signal. Dowsampling also exhibits a denoising effect, needing more components than the non-percolating methods. For the HCP dataset, the denoising effect is subtle, given that we do not have access to noiseless signals. Downsampling and Random projections find a plateau in the relative distortion (RD) curve, meaning that the signal has a low entropy that is captured with only few components. In both datasets, dimensionality reduction by random projections and random sampling fail to diminish the noise component, this is due to their property to maintain approximate distance, representing also the noise.

Percolation behavior: Given that percolation is characterized by the occurrence of one huge cluster for mild or large k values, we monitored the size of the largest cluster when varying the number k of clusters.

The results of tracking the size of the largest cluster are presented in Fig. 8 (*bottom*). This shows that among the traditional agglomerative methods, single, average and complete linkage display the worst behavior with a persistent percolation. Complete-linkage exhibits a more complex behavior, with the occurrence of relatively large clusters in the large k regime, that grows slowly in the small k regime. On the other hand, Ward and SLIC are the most resilient methods to percolation, both known for their tendency

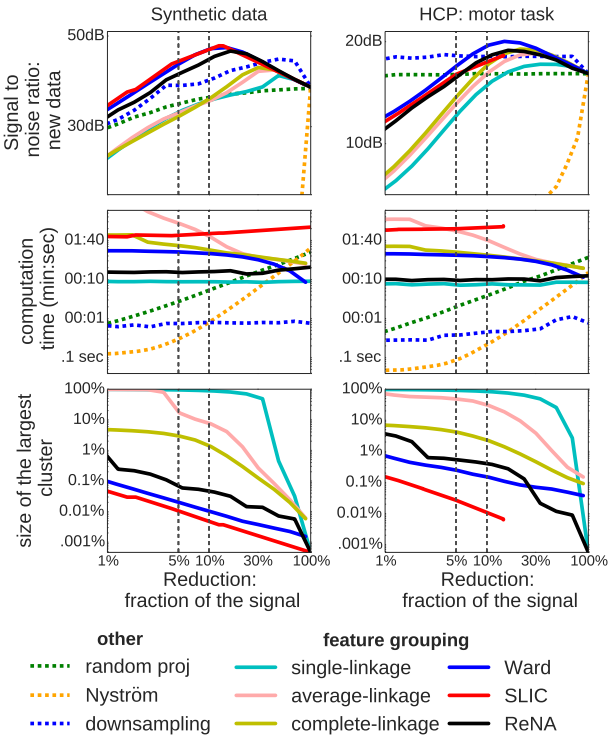

Figure 8. **Quality assessment of various approximation techniques on synthetic and brain imaging data:** Evaluation of the performance for several number k of clusters. *(top)* Empirical measure of the distortion, RD of the approximated distance. For a fraction of the signal between 5% and 30% Ward, SLIC and ReNA present a denoising effect, improving the approximation of the distances. In contrast, traditional agglomerative clustering fails to preserve the distance in the reduced space. Downsampling displays an intermediate performance. *(center)* Regarding computation time, downsampling and random sampling outperform all the alternatives, followed by random projections and single-linkage. The proposed method is almost as fast as single-linkage. *(bottom)* Percolation behavior, obtained through the size of the largest cluster. Ward, SLIC and ReNA are the best avoiding huge clusters. The vertical dashed lines indicate the useful value range for practical applications ($k \in [\lfloor p/20 \rfloor, \lfloor p/10 \rfloor]$).

to create equally large clusters. Finally, ReNA achieves a slightly worst performance, but mostly avoids huge clusters. The results are again across both datasets.

Computation time: Computation-time of the different methods are displayed in Fig.8 (*center*). Dimension reduction by downsampling is overall fastest, as it does not require any training and the computational time lies in the linear interpolation. It is followed by the Nyström approximation, with faster computation for a small number k of components. While computation time of Nyström approximation and random projections increases with the reduction fraction of signal, clustering algorithms are faster, as they require less merges. Random projections are faster then clustering approaches to reduce signals to a size smaller than 30% of their original size. In the clustering approaches, single-linkage and ReNA are the fastest, as expected. Note that the cost of the clustering methods scales linearly with the number of samples, hence can be reduced by subsampling: using less data to build the feature grouping.

4.4 Use in prediction tasks

To evaluate the denoising properties of dimension reduction, we now consider there use in prediction tasks. We use linear estimators as they are standard in high dimensional large-scale problems. In particular, we focus on linear estimators with ℓ_2 or ℓ_1 penalties. For ℓ_2 case, the estimation problem $\mathbf{\Phi}_{\mathsf{FG}}^{\mathsf{T}}\mathbf{\Phi}_{\mathsf{FG}}$ acts like a kernel of the quadratic form. For such estimators, dimension reductions that preserve pairwise distance are well theoretically motivated [14]

For each problem, we use the relevant metric (i.e. explained variance[9] for regression and accuracy[10] for classification) to assess the performance with different dimension reduction methods, as each one yields a different estimator. These results are then compared with those obtained based on raw data.

4.4.1 *Spatial approximation on a faces recognition task*

Face recognition is a classic computer-vision task. A standard pipeline to tackle this problem consists of dimensionality reduction of the data and then training a classifier to recognize an unseen face image. Some of the pipelines include random projections, PCA, downsampling [44] or dictionary learning [52]. It has been shown that images of a subject with a fixed pose and varying illumination lie close to a low-dimensional subspace [53]. This justifies the use of data approximation, in particular with linear projections.

To perform the classification task, we use an ℓ_2 or ℓ_1 logistic regression with a multi class *one-vs-rest* strategy and set the regularization parameter λ by 10-fold nested cross-validation. We mimic a study on reduced face representations [44], computing prediction accuracy for various feature-space dimensions $k \in \{30, 56, 120, 504\}$, corresponding to downsampling ratios of $\{1/32, 1/24, 1/16, 1/8\}$ respectively. Prediction error is measured in 50 iterations of a cross-validation loop randomly selecting half of images in each subject for the training and the other half for testing.

Fig. 9 reports the prediction accuracies. For high reduction factors ($k = 30$), Ward, Nyström, and ReNA perform up to 10% better than random projections or downsampling: representations adjusted on the data outperform data-independent reduction operators. For raw data, without reduction, prediction accuracy is around 95.3% and 94.1% for the ℓ_1 and ℓ_2 penalization respectively. Similar performance is obtained after reducing the signal by a factor of 64 with random projections, Nyström, downsampling, Ward, SLIC or ReNA. In contrast, single, average and complete linkage clustering fail to achieve the same performance. This shows the importance of finding balanced clusters.

Regarding computation time, data reduction speeds up the convergence of the logistic regression. Nyström and downsampling are the fastest methods. They are followed by random projections, single-linkage and ReNA, all of them having similar performances. Average, complete linkage, Ward and SLIC are slightly slower on this dataset.

4.4.2 *Convergence time: a good solution on a time budget*

We now turn to evaluating dimension reduction on brain imaging data. Machine learning techniques is often used on

9. The explained variance is defined as $R^2 = 1 - \frac{\mathrm{Var(model - signal)}}{\mathrm{Var(signal)}}$
10. Accuracy is defined by: $1 - \frac{\text{number of miss-classifications}}{\text{total number of samples}}$

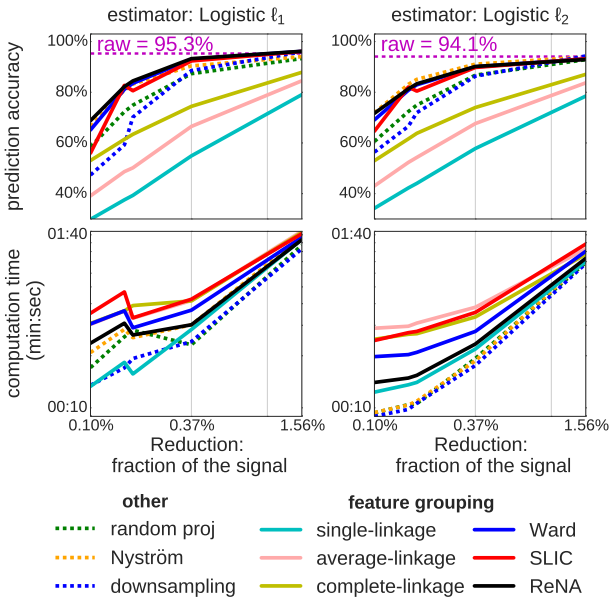

Figure 9. **Impact on face prediction accuracy for various approximation schemes:** Prediction accuracy as function of the feature space dimension obtained for various approximation schemes and classifiers for the recognition of human identities on the extended Yale B dataset. The clustering methods finding balanced clusters need less features to have a fair performance, and they also obtain significantly higher scores than the percolating methods.

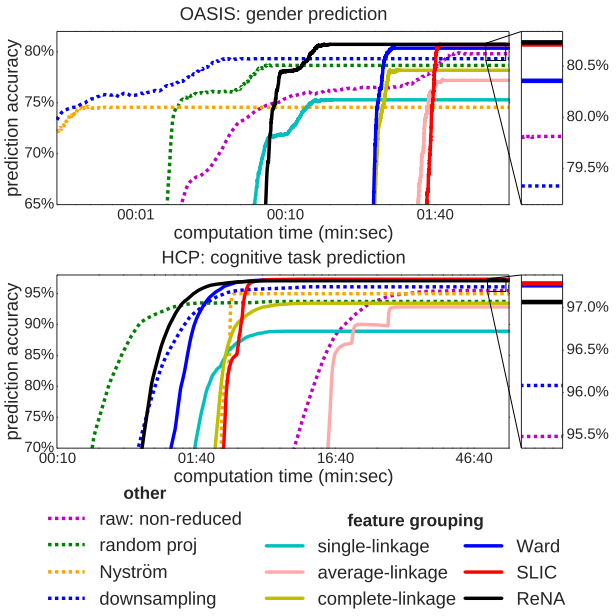

Figure 10. **Computation time taken to reach a solution:** Quality of the fit of a ℓ_2 penalized logistic regression as function of the computation time for a fixed number of clusters. In both datasets, Ward, SLIC and ReNA obtain significantly higher scores than estimation on non-reduced data with less computation time to reach a stable solution. Note that the time displayed does include cluster computation.

brain images to link brain regions with external variables (e.g. experiment conditions or cognitive tasks) [54], [55]. Linear models are generally used as their coefficients form brain maps that can be interpreted [56]. With progress in MRI, brain images are becoming bigger, leading to computational bottlenecks. The Human Connectome Project (HCP) is prototypical of these challenges, scanning 1 200 subjects with high-resolution protocols. We consider two brain-imaging prediction problems: *i)* gender classification using anatomical brain images of the 400 subjects from OASIS dataset and *ii)* the prediction of 17 cognitive tasks using functional brain images from 483 subjects of the HCP dataset. Here we study how dimension reduction can speed up convergence of classifiers. To do so, we measure the computation time needed to reach a stable solution for an ℓ_2 logistic regression, including the cost of computing the compressed representation and of training the classifier. We using a multinomial logistic regression with an ℓ_2 penalty and an L-BFGS-based solver.

In Fig. 10, we report prediction results as a function of computing time on the OASIS and HCP dataset. In both datasets, feature clustering with single, average, and complete linkage lead to poor prediction. This was expected due their tendency to find unbalanced clusters (percolation). On the other hand, Ward, SLIC, and ReNA obtain better prediction accuracy than raw data. All three approaches converge to similar accuracies, though with different convergence time. On the HCP dataset, SLIC takes more time to find the clusters, but it requires only a few iterations to converge, likely because it finds good quality clusters. Downsampling displays uneven performance, on the HCP dataset it performs slightly better than raw, while performing marginally worst on the OASIS dataset. In both datasets, the Nyström approximation and random projection achieve a lower prediction level than raw, this is because these methods capture both data and noise.

Improved performance of feature clustering compared to raw data highlights the importance of its signal denoising effect. ReNA strikes an excellent balance, as it reaches accuracies above that of raw data fastest.

4.4.3 *Impact of approximation on prediction accuracy*

Here, we examine the impact of the signal approximation on prediction accuracy. We use various datasets (i.e. faces, anatomical and functional brain images), setting $k = \lfloor p/20 \rfloor$ for random projections, downsampling and clustering methods, and $k = \lfloor n/10 \rfloor$ for Nyström. For the faces dataset, we use the $k = 504$ for all the methods; this value corresponds to a downsampling ratio of $1/8$. In addition, we predict age on the OASIS dataset, using a Ridge regression and setting its regularization parameter via cross validation. For each prediction task, we measure for all dimension reduction schemes the prediction accuracy, relatively to the mean prediction with raw data.

Fig. 11 summarizes the impact of dimension reduction on prediction accuracy and computation time. Dimension reduction with clustering algorithms that yield balanced clusters (Ward, SLIC, and ReNA) achieve similar or better accuracy as with raw data while bringing drastic time savings. Random projections and the percolating methods give consistently worse prediction accuracy than raw data. On the OASIS dataset, downsampling, SLIC, and Ward achieve the same prediction accuracy as raw, and perform better than raw on other datasets. Nyström only performs as good as raw data on the faces dataset with an ℓ_2 penalized logistic

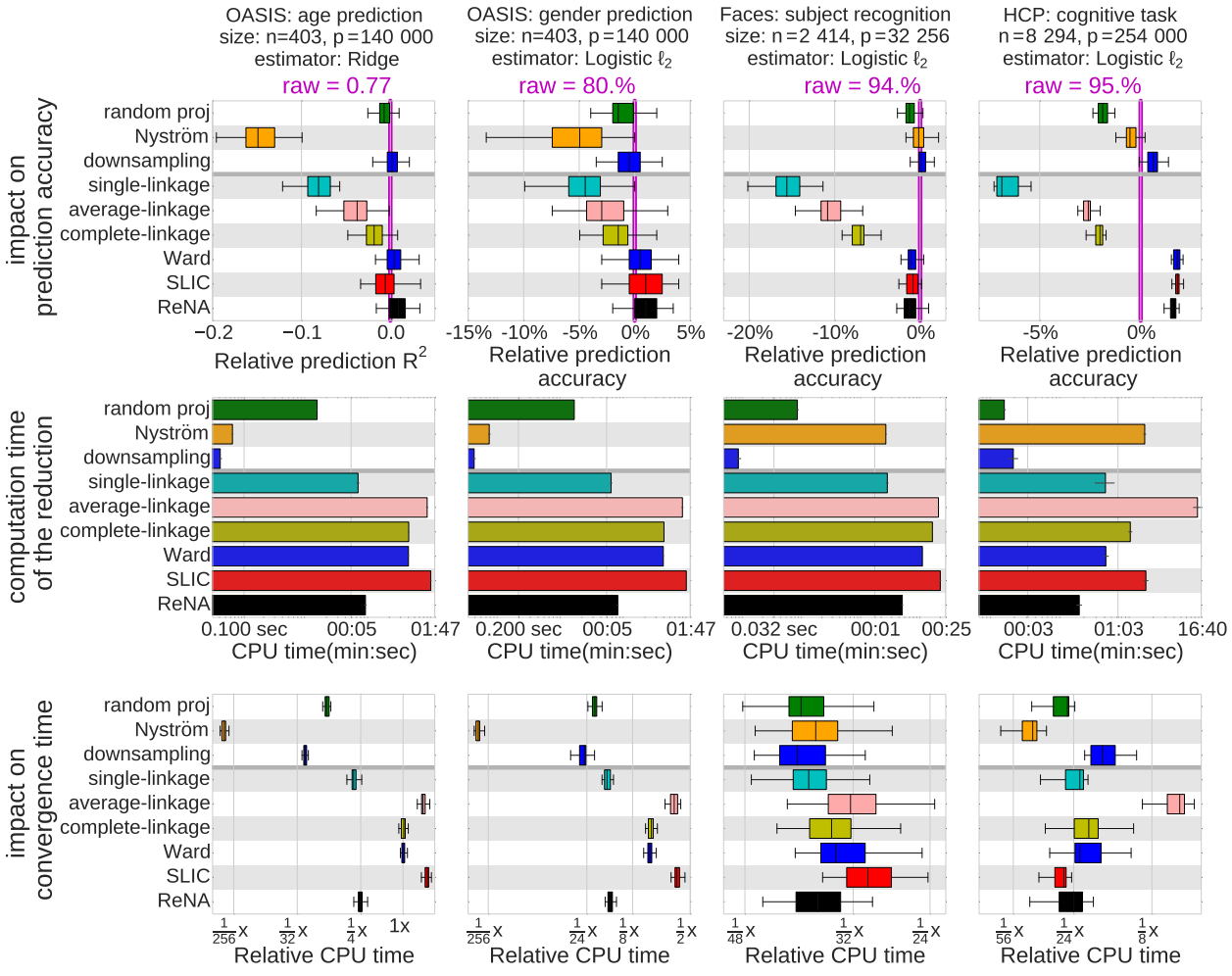

Figure 11. **Impact of reduction methods on prediction for various datasets:** *(Top)* Each bar represents the impact of the corresponding option on the prediction accuracy, relatively to the mean prediction with non-reduced data. Downsampling has the same performance as raw data. On the other hand, random projections, Nyström, single, average and complete linkage algorithms are consistently the worst ones across datasets. Ward, SLIC and ReNA perform at least as good as non-reduced data. *(middle)* Regarding the computation time to find a reduction, single-linkage and ReNA are consistently the best among the clustering algorithms. Random projections perform better than Nyström when the number of samples is large. Downsampling is the fastest across datasets. *(Bottom)* The time to converge for single-linkage and ReNA is almost the same. Average, complete-linkage and Ward are consistently the slowest. SLIC performs well on large datasets. Nyström and random projections are the fastest across datasets. Single-linkage and ReNA are the fastest clustering methods. ReNA strikes a good trade off between time and prediction accuracy.

regression. ReNA has a slightly worst performance than raw only in this dataset, and displays a better performance than raw on the remaining datasets (p-value $< 10^{-4}$). This illustrates the reduction of the spatial noise exhibited by non-percolating clustering methods.

4.5 Use in a spatial ICA task

Aside from the ℓ_1-penalized estimator, the data processing steps studied above depend only on the pairwise distances between samples. We now we investigate dimension reduction before an Independent Component Analysis (ICA), which probes higher moments of the data distribution. We use ICA on resting-state fMRI from the HCP dataset. ICA is used routinely on rest fMRI to separate signal from noise and obtain a spatial model of the functional connectome [57]. We use 93 subjects, with two resting-state fMRI sessions, each containing 1200 brain images.

We compare ICA on the raw data and after dimension reduction to five percent of the number of voxels ($k = \lfloor \frac{p}{20} \rfloor$). For the Nyström method the dimension is set to ten percent of the number n of samples ($k = \lfloor \frac{n}{10} \rfloor$). In each subject, we extract 40 independent components as it is a standard number in the literature. We investigate *i)* how similar the components obtained are before and after reduction; *ii)* how similar the components of session 1 and session 2 are with different reduction approaches. This second experiment gives a measure of the variability due to noise. In both cases, we measure similarity between components with the absolute value of their correlation, and match them across sessions with the Hungarian algorithm.

Fig. 12 summarizes the use of dimension reduction in ICA of rest fMRI. We find that the 40 components are highly similar before and after data reduction with downsampling and Ward: the average absolute correlation greater than 0.8. SLIC and ReNA have a slightly worst performance, with an average correlation greater than 0.74. On the other hand, single-linkage, average-linkage, complete-linkage, Nystöm, and random projections do not recover the components

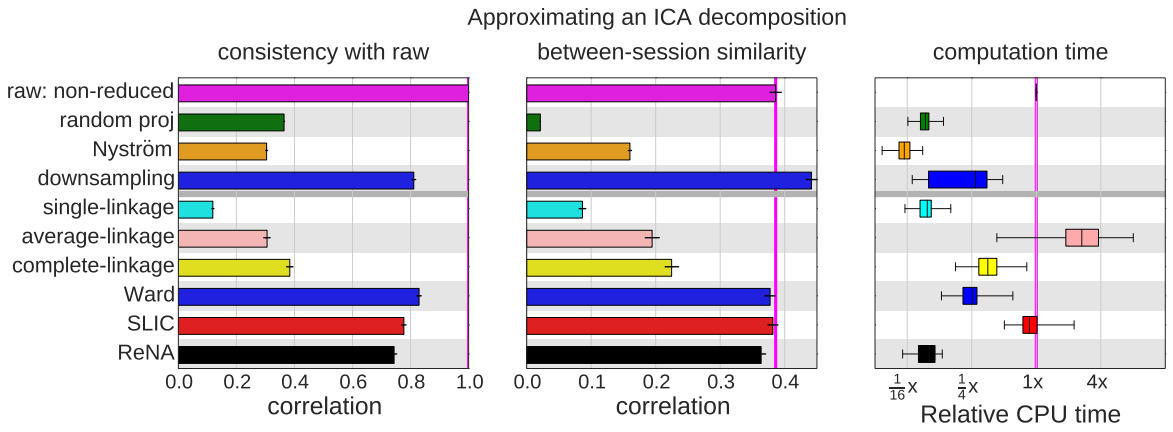

Figure 12. **Reproducibility of a spatial ICA after dimension reduction:** Reproducibility of 40 spatial independent components on 93 individual functional brain images dataset, with a fixed reduced dimension (see section 4.5). *(Left)* the reproducibility of downsampling, Ward, SLIC and ReNA with respect the non-compressed components is high. *(Middle)* across two sessions, donwsampling yields components more consistent than raw data. Ward, SLIC and ReNA perform as good as raw data, while other approaches fail to do so. *(Right)* regarding computational time, ReNA outperforms downsampling, Ward and SLIC, with a performance similar to single-linkage and random projections. It yields a gain factor of 16 with respect to raw data.

(average correlation < 0.4). As expected, the components between sessions obtained by non-percolating clustering (Ward, SLIC, and ReNA) are similar to the original ones. Donwsampling improves the similarity with respect to raw: the estimation problem is simpler and less noisy. On the opposite, single, average, and complete linkage yield a degradation of the similarity. This is caused by their tendency to percolate, hence dismiss information. Random projections and Nyström perform poorly. Indeed, they average data across the images, destroying the high-order moments of the data by creating signals more Gaussian than the originals. As a consequence, ICA cannot recover the sources derived from the original data. By contrast, the non-percolating clustering algorithms extract local averages of the data, that preserve its non-Gaussianity, as it has a spatial structure. Hence the spatial ICA is successful even though it has access to less samples. Finally, dimensionality reduction using ReNA speeds up the total analysis by a factor of 15.

5 Summary and Discussion

Fast dimension reduction is a crucial tool to tackle the rapid growth in datasets size, sample-wise and feature-wise. In particular, grouping features is natural when there is an underlying regularity in the observed signal, such as spatial structure in images or a more general neighborhood structure connecting features. We studied here a data-driven approach to feature grouping, where groups are first learned from a fraction of the data using a clustering algorithm, then used to build a compressed representation for further analysis.

We showed that feature grouping can preserve well the pairwise Euclidean distances between images. This property makes it well suited for ℓ_2-based algorithms, like shift-invariant kernel-based methods, or to approximate queries in information-retrieval settings. We also clarified under which hypotheses this scheme leads to a beneficial bias/variance compromise: as clustering adapts to the data, it reaches more optimal regimes than simple downsampling-based compression.

Additionally, we proposed a linear-time graph-structured clustering algorithm, ReNA, that is efficient with many clusters. This algorithm iteratively performs 1-nearest neighbor grouping, reduces the graph at each iteration, then averages the input features and repeats the process until it reaches the desired number of clusters. We have shown empirically that it is fast, does not percolate, and provides excellent performance in feature grouping for dimension reduction of structured data.

Our experiments have shown that on moderate-to-large datasets, non-percolating feature-grouping schemes (i.e. Ward, SLIC, and ReNA) most often outperform state-of-the-art fast data-approximation approaches for machine learning, namely random projection and random sampling. Using these methods in a predictive pipeline increases the quality of statistical estimations: they yield more accurate predictions than using all features. This indicates that feature grouping leads to a good approximation of the data, capturing the structure and reducing the noise. This denoising is due to the smoothness of the signal of interest: unlike the noise, the signal displays structure captured by feature grouping.

A key benefit of the ReNA clustering algorithm is that it is very fast while avoiding percolation. As a result, it gives impressive speed-ups for real-world multivariate statistical problems: often more than one order of magnitude. Note that the computational cost of ReNA is linear in the number of samples, hence additional computation gains can be obtained by sub-sampling its training data, as in Nyström approaches. In this work, we did not investigate the optimal choice of the number k of clusters, because we do not view compressed representations as a meaningful model per se, but as an approximation to reduce data dimension without discarding too much information. The range $k \in \left[\lfloor \frac{p}{20} \rfloor, \lfloor \frac{p}{10} \rfloor\right]$ is a useful regime it gives a good trade-off between computational efficiency and data fidelity. In our experiments, $k = \lfloor \frac{p}{20} \rfloor$ gave enough data fidelity for statistical analysis to perform at least as good as raw data. In this regime, Ward clustering gives slightly better

approximations of the original data, however it is slower, often by several factors, hence is not a practical solution.

We have shown that feature grouping is useful beyond ℓ_2-distance-based methods: it also gives good performance on estimators relying on higher order moments (e.g. ICA) or sparsity (ℓ_1-based regression or classification)[11]. As future work, it would be interesting to investigate the use of ReNA-based feature grouping in expensive sparse algorithms, for instance with sparse dictionary learning, where feature subsampling can give large speed ups [58]. Similarly, the combination of clustering, randomization, and sparsity has also been shown to be an effective regularization for some ill-posed inverse problems [59] [30]. We conjecture that ReNA clustering is particularly well-suited for these problems. This is all the more important that computation cost is a major roadblock to the adoption of such estimators.

An important aspect of feature grouping compared to other fast dimension reductions, such as random projections, is that the features of the reduced representation it creates of the data make sense for the application. Consequently, the dimension reduction step can be inverted, and any statistical analysis performed after reduction can be reported with regard to the original signal.

Given that ReNA clustering is extremely fast, the proposed featuring-grouping is an extremely promising avenue to speed up any statistical analysis of large datasets where the information is in the large-scale structure of the signal. Such approach is crucial for domains where the resolution of the sensors is rapidly increasing, in medical or biological imaging, genomics or geospatial data.

ACKNOWLEDGMENTS

Data were provided in part by the Human Connectome Project, WU-Minn Consortium (Principal Investigators: David Van Essen and Kamil Ugurbil; 1U54MH091657) funded by the 16 NIH Institutes and Centers that support the NIH Blueprint for Neuroscience Research; and by the McDonnell Center for Systems Neuroscience at Washington University. The research leading to these results has received funding from the European Union Seventh Framework Programme (FP7/2007-2013) under grant agreement N°604102 (HBP)

REFERENCES

[1] F. Amat, E. W. Myers, and P. J. Keller, "Fast and robust optical flow for time-lapse microscopy using super-voxels," *Bioinformatics*, vol. 29, pp. 373–80, 2013.

[2] D. V. Essen, K. Ugurbil, E. Auerbach, D. Barch, T. Behrens, R. Bucholz, A. Chang, L. Chen, M. Corbetta, S. Curtiss, S. D. Penna, D. Feinberg, M. Glasser, N. Harel, A. Heath, L. Larson-Prior, D. Marcus, G. Michalareas, S. Moeller, R. Oostenveld, S. Petersen, F. Prior, B. Schlaggar, S. Smith, A. Snyder, J. Xu, and E. Yacoub, "The human connectome project: A data acquisition perspective," *NeuroImage*, vol. 62, pp. 2222–2231, 2012.

[3] R. Overbeek, N. Larsen, G. D. Pusch, M. DâĂŹSouza, E. S. Jr, N. Kyrpides, M. Fonstein, N. Maltsev, and E. Selkov, "Wit: integrated system for high-throughput genome sequence analysis and metabolic reconstruction," *Nucleic Acids Research*, vol. 28, pp. 123–125, 2000.

11. On the faces datasets for the ℓ_1 estimator, ReNA performs as well as raw data.

[4] J. R. Cole, Q. Wang, J. A. Fish, B. Chai, D. M. McGarrell, Y. Sun, C. T. Brown, A. Porras-Alfaro, C. R. Kuske, and J. M. Tiedje, "Ribosomal database project: data and tools for high throughput rrna analysis," *Nucleic Acids Research*, 2013.

[5] T. Addair, D. Dodge, W. Walter, and S. Ruppert, "Large-scale seismic signal analysis with hadoop," *Computers & Geosciences*, vol. 66, p. 145, 2014.

[6] H. Jégou, M. Douze, and C. Schmid, "Improving bag-of-features for large scale image search," *International Journal of Computer Vision*, vol. 87, pp. 316–336, 2010.

[7] A. Rinaldo, S.-A. Bacanu, B. Devlin, V. Sonpar, L. Wasserman, and K. Roeder, "Characterization of multilocus linkage disequilibrium," *Genetic epidemiology*, vol. 28, p. 193, 2005.

[8] A. Dehman, C. Ambroise, and P. Neuvial, "Performance of a blockwise approach in variable selection using linkage disequilibrium information," *BMC bioinformatics*, vol. 16, p. 1, 2015.

[9] A. Hoyos-Idrobo, Y. Schwartz, G. Varoquaux, and B. Thirion, "Improving sparse recovery on structured images with bagged clustering," *IEEE PRNI*, 2015.

[10] A. Lucchi, K. Smith, R. Achanta, G. Knott, and P. Fua, "Supervoxel-based segmentation of mitochondria in em image stacks with learned shape features," *IEEE transactions on medical imaging*, vol. 31, no. 2, pp. 474–486, 2012.

[11] H. Wang and P. A. Yushkevich, "Multi-atlas segmentation without registration: a supervoxel-based approach," in *International Conference on Medical Image Computing and Computer-Assisted Intervention*. Springer, 2013, pp. 535–542.

[12] E. Keogh, K. Chakrabarti, M. Pazzani, and S. Mehrotra, "Dimensionality reduction for fast similarity search in large time series databases," *Knowledge and information Systems*, vol. 3, p. 263, 2001.

[13] K. Chakrabarti, E. Keogh, S. Mehrotra, and M. Pazzani, "Locally adaptive dimensionality reduction for indexing large time series databases," *ACM Trans. Database Syst.*, vol. 27, pp. 188–228, 2002.

[14] A. Rahimi and B. Recht, "Random features for large-scale kernel machines," in *NIPS*, 2007.

[15] N. Ailon and B. Chazelle, "The fast johnson-lindenstrauss transform and approximate nearest neighbors," *SIAM J. Comput.*, vol. 39, pp. 302–322, 2009.

[16] N. Halko, P. G. Martinsson, and J. A. Tropp, "Finding structure with randomness: Probabilistic algorithms for constructing approximate matrix decompositions," *SIAM Rev.*, vol. 53, pp. 217–288, 2011.

[17] D. I. Shuman, S. K. Narang, P. Frossard, A. Ortega, and P. Vandergheynst, "The emerging field of signal processing on graphs: Extending high-dimensional data analysis to networks and other irregular domains," *Signal Processing Magazine, IEEE*, vol. 30, pp. 83–98, 2013.

[18] A. Gittens and M. W. Mahoney, "Revisiting the nystrom method for improved large-scale machine learning." in *ICML*, 2013, pp. 567–575.

[19] M. W. Mahoney and P. Drineas, "Cur matrix decompositions for improved data analysis," *PNAS*, vol. 106, pp. 697–702, 2009.

[20] W. Johnson and J. Lindenstrauss, "Extensions of Lipschitz mappings into a Hilbert space," in *Conference in modern analysis and probability*, ser. Contemporary Mathematics. American Mathematical Society, 1984, vol. 26, pp. 189–206.

[21] J. Lin, E. Keogh, L. Wei, and S. Lonardi, "Experiencing sax: a novel symbolic representation of time series," *Data Mining and knowledge discovery*, pp. 107–144, 2007.

[22] D. Stauffer and A. Aharony, *Introduction to Percolation Theory*. Oxford University Press, New York, 1971.

[23] C. Hedge, A. C. Sankaranarayanan, W. Yin, and R. G. Baraniuk, "Numax: a convex approach for learning near-isometric linear embeddings," *IEEE Trans. Signal Process.*, vol. 63, pp. 6109–6121, 2015.

[24] Y. Lu, P. S. Dhillon, D. P. Foster, and L. H. Ungar, "Faster ridge regression via the subsampled randomized hadamard transform." in *NIPS*, 2013, pp. 369–377.

[25] D. Achlioptas, "Database-friendly random projections: Johnson-lindenstrauss with binary coins," *Journal of Computer and System Sciences*, vol. 66, pp. 671–687, 2003.

[26] J. A. Tropp, "Improved analysis of the subsampled randomized hadamard transform," 2011.

[27] R. G. Baraniuk and M. B. Wakin, "Random projections of smooth manifolds," *Found. Comput. Math.*, vol. 9, pp. 51–77, 2009.

[28] C. Williams and M. Seeger, "Using the nyström method to speed up kernel machines," in *NIPS*, 2001, pp. 682–688.

[29] A. Rudi, R. Camoriano, and L. Rosasco, "Less is more: NystrÃűm computational regularization," in *NIPS*, 2015, pp. 1648–1656.

[30] P. Bühlmann, P. Rütimann, S. van de Geer, and C.-H. Zhang, "Correlated variables in regression: clustering and sparse estimation," *Journal of Statistical Planning and Inference*, vol. 143, pp. 1835–1871, 2013.

[31] L. Le Magoarou and R. Gribonval, "Flexible multi-layer sparse approximations of matrices and applications," *arXiv preprint arXiv:1506.07300*, 2015.

[32] R. Achanta, A. Shaji, K. Smith, A. Lucchi, P. Fua, and S. Süsstrunk, "SLIC superpixels compared to state-of-the-art superpixel methods," *IEEE Trans. Pattern Anal. Mach. Intell.*, vol. 34, pp. 2274–2282, 2012.

[33] D. Arthur and S. Vassilvitskii, "How slow is the k-means method?" in *Annual Symposium on Computational Geometry*, 2006, p. 144.

[34] T. Hastie, R. Tibshirani, and J. Friedman, *The Elements of Statistical Learning*, 2nd ed., ser. Springer Series in Statistics. New York, NY, USA: Springer New York Inc., 2009.

[35] J. H. Ward, "Hierarchical grouping to optimize an objective function," *Journal of the American Statistical Association*, vol. 58, p. 236, 1963.

[36] D. Müllner, "Modern hierarchical, agglomerative clustering algorithms," *ArXiv e-prints*, 2011.

[37] M. Penrose, "Single linkage clustering and continuum percolation," *Journal of Multivariate Analysis*, vol. 53, pp. 94 – 109, 1995.

[38] B. Thirion, G. Varoquaux, E. Dohmatob, and J.-B. Poline, "Which fmri clustering gives good brain parcellations?" *Frontiers in Neuroscience*, vol. 8, 2014.

[39] P. F. Felzenszwalb and D. P. Huttenlocher, "Efficient graph-based image segmentation," *Int. J. Comput. Vision*, vol. 59, pp. 167–181, 2004.

[40] D. Eppstein, M. S. Paterson, and F. Yao, "On nearest-neighbor graphs". discrete and computational geometry," vol. 17, pp. 263–282, 1997.

[41] M. Ester, H. peter Kriegel, J. Sander, and X. Xu, "A density-based algorithm for discovering clusters in large spatial databases with noise." AAAI Press, 1996, pp. 226–231.

[42] S.-H. Teng and F. F. Yao, "k-nearest-neighbor clustering and percolation theory," *Algorithmica*, vol. 49, pp. 192–211, 2007.

[43] D. J. Pearce, "An improved algorithm for finding the strongly connected components of a directed graph," Tech. Rep., 2005.

[44] J. Wright, A. Yang, A. Ganesh, S. Sastry, and Y. Ma, "Robust face recognition via sparse representation," *IEEE Trans. Pattern Anal. Mach. Intell.*, vol. 31, pp. 210–227, 2009.

[45] D. S. Marcus, T. H. Wang, J. Parker, J. G. Csernansky, J. C. Morris, and R. L. Buckner, "Open access series of imaging studies (oasis): cross-sectional mri data in young, middle aged, nondemented, and demented older adults." *J Cogn Neurosci*, vol. 19, pp. 1498–1507, 2007.

[46] W. Chau and A. R. McIntosh, "The talairach coordinate of a point in the {MNI} space: how to interpret it," *NeuroImage*, vol. 25, pp. 408–416, 2005.

[47] D. M. Barch, G. C. Burgess, M. P. Harms, S. E. Petersen, B. L. Schlaggar, M. Corbetta, M. F. Glasser, S. Curtiss, S. Dixit, C. Feldt, D. Nolan, E. Bryant, T. Hartley, O. Footer, J. M. Bjork, R. Poldrack, S. Smith, H. Johansen-Berg, A. Z. Snyder, D. C. V. Essen, and W. U.-M. H. Consortium, "Function in the human connectome: task-fmri and individual differences in behavior." *Neuroimage*, vol. 80, pp. 169–189, 2013.

[48] M. F. Glasser, S. N. Sotiropoulos, J. A. Wilson, T. S. Coalson, B. Fischl, J. L. Andersson, J. Xu, S. Jbabdi, M. Webster, and J. R. Polimeni, "The minimal preprocessing pipelines for the human connectome project," *Neuroimage*, vol. 80, pp. 105–124, 2013.

[49] F. Pedregosa, G. Varoquaux, A. Gramfort, V. Michel, B. Thirion, O. Grisel, M. Blondel, P. Prettenhofer, R. Weiss, V. Dubourg, J. Vanderplas, A. Passos, D. Cournapeau, M. Brucher, M. Perrot, and E. Duchesnay, "Scikit-learn: Machine learning in Python," *Journal of Machine Learning Research*, vol. 12, p. 2825, 2011.

[50] S. van der Walt, J. L. Schönberger, J. Nunez-Iglesias, F. Boulogne, J. D. Warner, N. Yager, E. Gouillart, T. Yu, and the scikit-image contributors, "scikit-image: image processing in Python," *PeerJ*, vol. 2, p. e453, 2014.

[51] H. G. Katzgraber, "Random numbers in scientific computing: An introduction," *CoRR*, vol. abs/1005.4117, 2010.

[52] Z. J. Xiang, H. Xu, and P. J. Ramadge, "Learning sparse representations of high dimensional data on large scale dictionaries," in *NIPS*, 2011, pp. 900–908.

[53] R. Basri and D. Jacobs, "Lambertian reflection and linear subspaces," *IEEE Trans. Pattern Anal. Mach. Intell.*, vol. 25, pp. 218–233, 2003.

[54] T. M. Mitchell, R. Hutchinson, R. S. Niculescu, F. Pereira, X. Wang, M. Just, and S. Newman, "Learning to decode cognitive states from brain images," *Machine Learning*, vol. 57, p. 145, 2004.

[55] Y. Schwartz, B. Thirion, and G. Varoquaux, "Mapping cognitive ontologies to and from the brain," in *NIPS*, 2013.

[56] T. Naselaris, K. N. Kay, S. Nishimoto, and J. L. Gallant, "Encoding and decoding in fmri," *Neuroimage*, vol. 56, pp. 400 – 410, 2011.

[57] S. M. Smith, C. F. Beckmann, J. Andersson, E. J. Auerbach, J. Bijsterbosch, G. Douaud, E. Duff, D. A. Feinberg, L. Griffanti, M. P. Harms, M. Kelly, T. Laumann, K. L. Miller, S. Moeller, S. Petersen, J. Power, G. Salimi-Khorshidi, A. Z. Snyder, A. T. Vu, M. W. Woolrich, J. Xu, E. Yacoub, K. UÄŞurbil, D. C. V. Essen, and M. F. Glasser, "Resting-state fmri in the human connectome project," *NeuroImage*, vol. 80, pp. 144–168, 2013.

[58] A. Mensch, J. Mairal, B. Thirion, and G. Varoquaux, "Dictionary learning for massive matrix factorization," *ICML*, 2016.

[59] G. Varoquaux, A. Gramfort, and B. Thirion, "Small-sample brain mapping: sparse recovery on spatially correlated designs with randomization and clustering," in *ICML*, 2012, p. 1375.